A&A 635, A58 (2020)
https://doi.org/10.1051/0004-6361/201937275

Astronomy & Astrophysics

Galactic archaeology with asteroseismic ages

II. Confirmation of a delayed gas infall using Bayesian analysis based on MCMC methods

E. Spitoni[1], K. Verma[1], V. Silva Aguirre[1], and F. Calura[2]

[1] Stellar Astrophysics Centre, Department of Physics and Astronomy, Aarhus University, Ny Munkegade 120, 8000 Aarhus C, Denmark
e-mail: spitoni@phys.au.dk
[2] I.N.A.F. – Osservatorio Astronomico di Bologna, Via Gobetti 93/3, 40129 Bologna, Italy

Received 6 December 2019 / Accepted 28 January 2020

ABSTRACT

Context. With the wealth of information from large surveys and observational campaigns in the contemporary era, it is critical to properly exploit the data to constrain the parameters of Galactic chemical evolution models and quantify the associated uncertainties.
Aims. We aim to constrain the two-infall chemical evolution models for the solar annulus using the measured chemical abundance ratios and seismically inferred age of stars in the APOKASC sample. Recently, in revised two-infall chemical evolution models, a significant delay of ∼4.3 Gyr has been invoked between the two episodes of gas accretion. In this work, we wish to test its robustness and statistically confirm and quantify the delay.
Methods. We took a novel approach, using Bayesian framework based on Markov chain Monte Carlo methods to fit the two-infall chemical evolution models to the data.
Results. In addition to fitting the data for stars in the APOKASC sample, our best fit models also reproduce other important observational constraints of the chemical evolution of the disk: i) present day stellar surface density; ii) present-day supernova and star formation rates; iii) the metallicity distribution function; and iv) solar abundance values. We find a significant delay between the two gas accretion episodes for various models explored with different values for the star formation efficiencies. The values for the delay lie in the range 4.5−5.5 Gyr.
Conclusions. The results suggest that the APOKASC sample carries the signature of a delayed gas-rich merger, with dilution being the main process determining the shape of low-α stars in the abundance ratios space.

Key words. Galaxy: abundances – Galaxy: evolution – ISM: general – asteroseismology – methods: statistical

1. Introduction

The purpose of Galactic archaeology is to unveil the formation and evolution of our Galaxy by interpreting signatures imprinted in the observed chemical abundances and kinematics of resolved stellar populations. This is typically done through the proper exploitation of the observational stellar data to constrain models of Galactic chemical evolution. The contemporary wealth of data from big surveys and observational campaigns, such as for example spectroscopic properties from the Apache Point Observatory Galactic Evolution Experiment project (APOGEE; Majewski et al. 2017), kinematic properties from the "fossil" record of old stellar populations as provided by the *Gaia* mission (DR2; Gaia Collaboration 2018), and precise seismic ages from the *Kepler* satellite (Borucki et al. 2009), offer an unprecedented opportunity to test models of galaxy formation and evolution.

The analysis of the APOGEE data (Nidever et al. 2014; Hayden et al. 2015) suggested the existence of a clear distinction between two sequences of disc stars in the [α/Fe] versus [Fe/H] abundance ratio space: the so-called high-α and low-α sequences. This dichotomy has also been confirmed by the *Gaia*-ESO survey (e.g. Recio-Blanco et al. 2014; Rojas-Arriagada et al. 2016, 2017) and the AMBRE project (Mikolaitis et al. 2017).

In several theoretical models of Galactic disc evolution it has been proposed that this bimodality is strictly connected to a delayed gas-accretion episode of primordial composition. For instance, a late second accretion phase after a prolonged period with a quenched star formation rate (SFR) has been suggested by the dynamical models presented by Noguchi (2018). Moreover, the AURIGA simulations presented by Grand et al. (2018) clearly point out that a bimodal distribution in the [Fe/H]-[α/Fe] plane is a consequence of a significantly lowered gas accretion rate at ages between 6 and 9 Gyr. In the framework of cosmological hydrodynamic simulations of Milky Way-like galaxies, Buck (2020) stated that a bimodal α-sequence is a generic consequence of a gas-rich merger at some time in a galaxy's evolution. As also suggested by Spitoni et al. (2019a), a merger gives rise to a low-α sequence by bringing pristine metal-poor gas into the system which dilutes the metallicity of interstellar medium while keeping [α/Fe] abundance almost unchanged (as first proposed in a cosmological model by Calura & Menci 2009).

The model presented by Spitoni et al. (2019a, hereafter ES19) also includes precise stellar ages provided by asteroseismology to constrain the chemical evolution of the solar neighbourhood. The ES19 model is an updated version of the classical "two-infall" model of Chiappini et al. (1997), in which an early fast gas accretion episode gives rise to the high-α

sequence, and at a later Galactic time, the low-α sequence is created by a different infall event characterised by a longer timescale of accretion. The predictions of the revised two-infall models were compared with the measured chemical abundance ratios (Pinsonneault et al. 2014) and seismically inferred age of stars in the APOKASC catalogue (APOGEE + *Kepler* Asteroseismology Science Consortium; Silva Aguirre et al. 2018). The ES19 model was capable of reproducing the APOKASC data assuming a disc component dissection based on chemistry (see Silva Aguirre et al. 2018), that is, the sample was divided into two distinct groups called "high-α" and "low-α" sequences. The most important result of ES19 was that a significant delay of ∼4.3 Gyr between the two infall episodes was required to reproduce the measured stellar abundances and seismically inferred ages.

In ES19, the choice of free parameters, that is, the two infall timescales, the corresponding star formation efficiencies, and the delay between the two infall episodes of the model was made to qualitatively reproduce the observed [α/Fe] versus [Fe/H] abundance ratios. In this article we present a quantitative study of the free parameters using a Bayesian analysis. Probabilistic data analysis has transformed scientific research in the past decade. In particular, Bayesian analysis based on Markov chain Monte Carlo (MCMC) methods has been used in several different areas of astrophysics including cosmology (Dunkley et al. 2005), cosmic rays (Putze et al. 2010), active galactic nuclei (Reynolds et al. 2012), Milky Way dwarf satellites (Ural et al. 2015), semi-analytical models of galaxy formation (Kampakoglou et al. 2008; Henriques et al. 2009, 2013), and stellar nucleosynthesis (Cescutti et al. 2018), among others. Recently, MCMC methods have been used to test Galactic chemical-evolution models (see e.g. Côté et al. 2017; Rybizki et al. 2017; Philcox et al. 2018; Frankel et al. 2018; Belfiore et al. 2019).

In this paper, we present the first attempt to perform a detailed study of the key parameters that regulate the evolution of the solar neighbourhood by means of a match between a Bayesian MCMC method and the two-infall chemical-evolution model. Our goal is to test the findings of ES19 by quantitatively inferring the delay between the two accretion episodes without imposing any stellar data separation based on chemical abundances.

The paper is organised as follows: in Sect. 2 the observational data used in the Bayesian analysis are presented, in Sect. 3 we briefly recall the main characteristics of two infall model, in Sect. 4 we describe the fitting method and also perform a preliminary test, in Sect. 5 we present our results, and finally in Sect. 6 we summarise our conclusions.

2. The APOKASC sample

In this work we use a Bayesian framework based on MCMC methods to fit state-of-the-art models of Galactic chemical evolution to the observed chemical abundance ratios and asteroseismic ages of stars in the updated APOKASC (APOGEE+ *Kepler* Asteroseismology Science Consortium) sample presented by Silva Aguirre et al. (2018).

The sample is composed by 1197 red giants spanning out to 2 kpc in the solar annulus with stellar properties determined combining the photometric, spectroscopic, and asteroseismic observables in the BAyesian STellar Algorithm (`BASTA`, Silva Aguirre et al. 2015, 2017) framework. The sample is also characterised by precise kinematic information available from the first data release (DR1) of *Gaia* (Lindegren et al. 2016; Gaia Collaboration 2016) and The Fourth US Naval Observatory CCD Astrograph (UCAC-4) catalogue (Zacharias et al. 2013). Here, it is assumed that α abundances are given by the sum of the individual Mg and Si abundances (Salaris et al. 2018).

As in ES19, in the present work we do not consider the so-called young α rich (YαR) stars. The origin of these stars is still uncertain and two different scenarios have been proposed: either they are objects migrated from the Galactic bar (Chiappini et al. 2015) or evolved blue stragglers (Martig et al. 2015; Chiappini et al. 2015; Yong et al. 2016; Jofré et al. 2016).

3. The revised two-infall model by ES19

In this section we reiterate the main assumptions and characteristics of the revised two-infall chemical evolution model proposed by ES19. A few details on the model are provided, including the parametrisation of the most basic physical processes (e.g. infall and star formation), as well as the stellar nucleosynthesis prescriptions used in the work.

3.1. The chemical evolution model prescriptions

In ES19 the authors revised the classical two-infall chemical evolution model in order to reproduce the data from the updated APOKASC catalogue by Silva Aguirre et al. (2018) which were chemically dissected into high-α and low-α stellar sequences. From the precise stellar ages determined via asteroseismology, a clear age difference emerged in the solar annulus between high-α and low-α stars. The low-α sequence age distribution peaks at ∼2 Gyr, whereas the high-α one peaks at ∼11 Gyr.

In ES19 the Milky Way disc is assumed to be formed by two distinct accretion episodes of gas. The gas infall rate is expressed by the following expression,

$$\mathcal{I}_i(t,i) = (X_i)_{\rm inf}\left[\mathcal{N}_1\, e^{-t/\tau_1} + \theta(t-t_{\rm max})\mathcal{N}_2\, e^{-(t-t_{\rm max})/\tau_2}\right], \quad (1)$$

where τ_1 is the timescale for the formation of the high-α sequence which was fixed at a value of 0.1 Gyr and τ_2 is the timescale for the formation of the low-α disc phase which was fixed at a value of 8 Gyr. We remind the reader that the θ in the equation above is the Heaviside step function. $(X_i)_{\rm inf}$ is the abundance by mass of the element i in the infalling gas which is assumed to have primordial composition, whereas $t_{\rm max} = 4.3$ Gyr is the time of the maximum infall rate on the second accretion episode, that is, it indicates the delay of the beginning of the second infall. Spitoni et al. (2019a) emphasised the importance of the $t_{\rm max}$ value in order to properly reproduce the APOKASC data. Finally, the coefficients $\mathcal{N}_1$ and $\mathcal{N}_2$ are obtained by imposing a fit to the observed current total surface mass density in the solar neighbourhood adopting the relations

$$\mathcal{N}_1 = \frac{\sigma_1}{\tau_1\left(1-e^{-t_{\rm G}/\tau_1}\right)}, \quad (2)$$

$$\mathcal{N}_2 = \frac{\sigma_2}{\tau_2\left(1-e^{-(t_{\rm G}-t_{\rm max})/\tau_2}\right)}, \quad (3)$$

where σ_1 and σ_2 are the present-day total surface mass density of the high-α and low-α sequence stars, respectively; $t_{\rm G}$ is the Age of the Milky Way.

The SFR is expressed as the Kennicutt (1998) law,

$$\psi(t) = \nu\sigma_g^k(t), \quad (4)$$

where ν is the star formation efficiency (SFE), σ_g is the surface gas density, and $k = 1.5$ is the exponent. In ES19 the adopted SFE is constant throughout the lifetime of the Galaxy and is fixed

at the value of $\nu = 1.3\,\mathrm{Gyr}^{-1}$. However, different infall episodes could in principle be characterised by different SFEs. In fact, in the two-infall model by Grisoni et al. (2017, 2018) the SFEs associated to the high- and low-α sequences are different: $\nu_1 = 2\,\mathrm{Gyr}^{-1}$ and $\nu_2 = 1\,\mathrm{Gyr}^{-1}$. We adopt the Scalo (1986) initial stellar mass function (IMF), constant in time and space.

3.2. Nucleosynthesis prescriptions and solar values

As for the nucleosynthesis prescriptions for Fe, Mg, and Si, ES19 adopted the ones suggested by François et al. (2004). For a detailed description we refer to ES19. This set of yields has been widely used in the literature (Cescutti et al. 2007; Spitoni & Matteucci 2011; Mott et al. 2013; Spitoni et al. 2015, 2017, 2019b; Vincenzo et al. 2019) and was found to be able to reproduce the main features of the solar neighbourhood. We have adopted the photospheric values of Asplund et al. (2005) as our solar reference abundances to be consistent with the APOGEE data release (García Pérez et al. 2016).

4. The fitting method

Bayesian analysis based on MCMC methods has transformed scientific research in the past decade. Since there are already several text books and reviews on Bayesian statistics (see e.g. Jaynes 2003; Gelman et al. 2013) and MCMC methods (see e.g. Brooks et al. 2011; Sharma 2017; Hogg & Foreman-Mackey 2018; Speagle 2019), we only describe them briefly and highlight the aspects specific to the problem at hand.

In the context of parameter estimation, Bayes' theorem provides a way to update the parameters based on any new available data. In other words, it enables the calculation of the posterior probability distribution of the parameters given the new data,

$$P(\mathbf{\Theta}|\mathbf{x}) = \frac{P(\mathbf{\Theta})}{P(\mathbf{x})} P(\mathbf{x}|\mathbf{\Theta}), \tag{5}$$

where $\mathbf{x}$ represents the set of observables, $\mathbf{\Theta}$ the set of model parameters, $P(\mathbf{x}|\mathbf{\Theta}) \equiv \mathscr{L}$ the likelihood (i.e. probability of observing the data given the model parameters), $P(\mathbf{\Theta})$ the prior (i.e. probability of the model parameters before seeing the data, $\mathbf{x}$), and $P(\mathbf{x})$ represents the evidence (i.e. total probability of observing the data). The evidence is a normalising constant and can be calculated by integrating the likelihood over all model parameters. In the current study, $\mathbf{x} = \{[\alpha/\mathrm{Fe}],\ [\mathrm{Fe/H}],\ \mathrm{age}\}$ and $\mathbf{\Theta} = \{\tau_1,\ \tau_2,\ t_{\max},\ \sigma_2/\sigma_1\}$ are examples of the set of observables and model parameters, respectively.

To define the likelihood in Eq. (5) we assume that the uncertainties on the observables are normally distributed. In that case, the logarithm of the likelihood can be written as,

$$\ln \mathscr{L} = -\sum_{n=1}^{\mathrm{N}} \ln\left((2\pi)^{\mathrm{d}/2} \prod_{j=1}^{\mathrm{d}} \sigma_{n,j} \right) - \frac{1}{2} \sum_{n=1}^{\mathrm{N}} \sum_{j=1}^{\mathrm{d}} \left(\frac{x_{n,j} - \mu_{n,j}}{\sigma_{n,j}} \right)^2, \tag{6}$$

where N is the number of stars in the sample and d is the number of available observables. The quantities $x_{n,j}$ and $\sigma_{n,j}$ are respectively the measured value of the jth observable and its uncertainty for the nth star. In principle, the quantity $\mu_{n,j}$ is the model value of the jth observable for the nth star; in practice however it is tricky to define (as explained below).

To define $\mu_{n,j}$, we first consider the case of fitting the data only in the [Fe/H]-[α/Fe] plane. As can be seen in Fig. 1, the curve predicted by the two-infall model in this plane is multivalued, that is, there is more than one value of [α/Fe] for certain values of [Fe/H]. As a result, it becomes ambiguous to associate an observed data point in the [Fe/H]-[α/Fe] plane to a point on the curve, making it difficult to define $\mu_{n,j}$. In this study, we associate a data point to the closest point on the curve. Given a data point $x_{n,j}$, this is done by defining the following function,

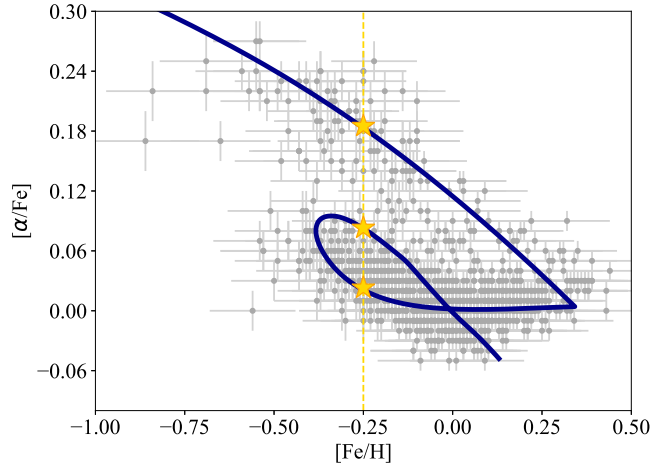

Fig. 1. Observed [α/Fe] vs. [Fe/H] abundance ratios of the APOKASC sample (grey points) presented by Silva Aguirre et al. (2018) compared with the two-infall chemical evolution model characterised by $\tau_1 = 0.1$ Gyr, $\tau_2 = 8$ Gyr, $\sigma_2 = 64\,M_\odot\,\mathrm{pc}^{-2}$, $\sigma_2/\sigma_1 = 4$, and $\nu = 1.3\,\mathrm{Gyr}^{-1}$. The three yellow points clearly show that the predicted chemical evolution curve is multi-valued in this plane (they exhibit three different [α/Fe] values for the same [Fe/H] abundance ratio).

$$S_n \equiv \min_i \left\{ \sqrt{\sum_{j=1}^{2} \left(\frac{x_{n,j} - \mu_{n,j,i}}{\sigma_{n,j}} \right)^2} \right\} = \sqrt{\sum_{j=1}^{2} \left(\frac{x_{n,j} - \mu_{n,j,i'}}{\sigma_{n,j}} \right)^2}, \tag{7}$$

where i runs over the different points on the curve. Hence, the closest point on the curve is $\mu_{n,j} = \mu_{n,j,i'}$. This definition can be easily generalised to define $\mu_{n,j}$ for an arbitrary number of observables by modifying Eq. (7),

$$S_n \equiv \min_i \left\{ \sqrt{\sum_{j=1}^{\mathrm{d}} \left(\frac{x_{n,j} - \mu_{n,j,i}}{\sigma_{n,j}} \right)^2} \right\} = \sqrt{\sum_{j=1}^{\mathrm{d}} \left(\frac{x_{n,j} - \mu_{n,j,i'}}{\sigma_{n,j}} \right)^2}. \tag{8}$$

The computation of the posterior also requires the specification of priors on the model parameters (see Eq. (5)). Here, we discuss the priors on $\mathbf{\Theta} = \{\tau_1,\ \tau_2,\ t_{\max},\ \sigma_2/\sigma_1\}$ and justify their choices in the current study.

- First infall timescale τ_1: in the classical two-infall model (Chiappini et al. 1997) the first gas infall is characterised by a short timescale of accretion and has been fixed at the value of $\tau_1 = 1$ Gyr. More recently, in order to reproduce the AMBRE thick disc, Grisoni et al. (2017) suggested a smaller value: $\tau_1 = 0.1$ Gyr. In the current study, we set a uniform prior on τ_1, exploring the range $0 < \tau_1 < 7$ Gyr.
- The second infall timescale, τ_2, is connected to a slower accretion episode. We set a uniform prior on τ_2 exploring the range $0 < \tau_2 < 28$ Gyr, since there is no reason for τ_2 to be limited to the age of the Universe.
- The delay $t_{\max}$: we set a uniform prior exploring the range $0 < t_{\max} < 14$ Gyr, which extends all the way to the age of the Universe.
- Present-day two-surface mass–density ratio, σ_2/σ_1: there are still large discrepancies in the estimates of the thick disc surface density quoted in the literature, which contribute to large

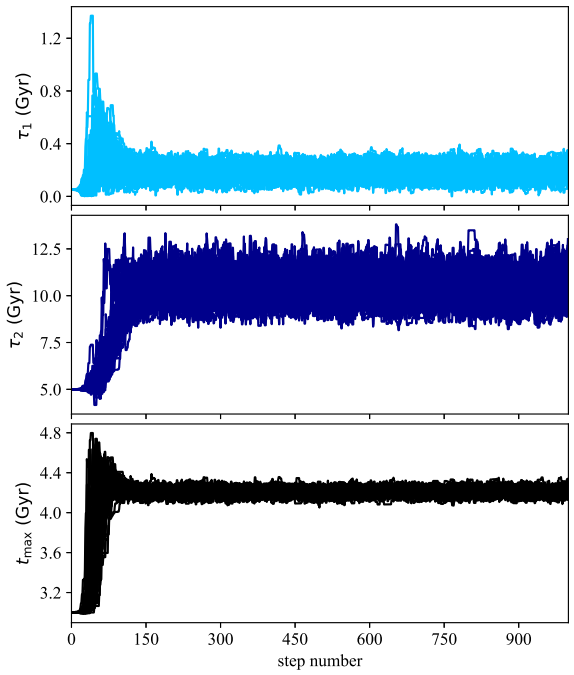

Fig. 2. Convergence of the three free model parameters composed by the set $\boldsymbol{\Theta} = \{\tau_1,\ \tau_2,\ t_{max}\}$ (see model details in Sect. 4) as a function of number of steps.

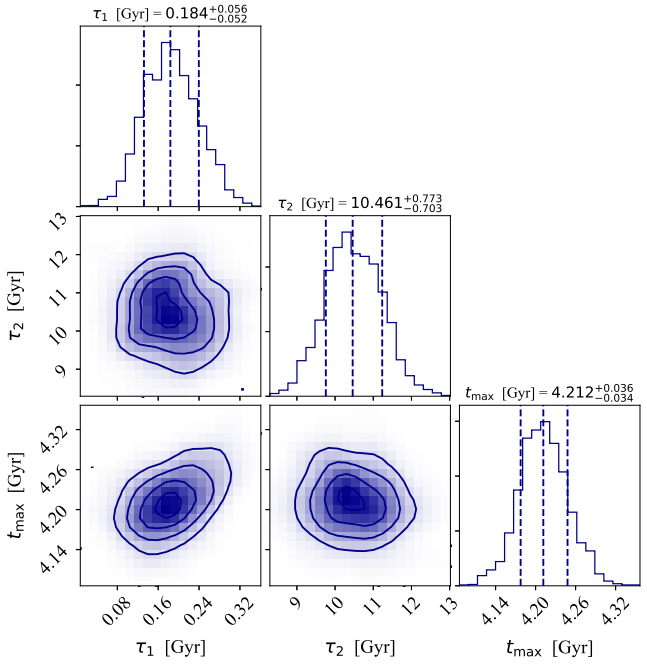

Fig. 3. Corner plot showing the posterior PDFs for the same model set as in Fig. 2 obtained by fitting [α/Fe] and [Fe/H] abundances from the Silva Aguirre et al. (2018) sample. For each parameter, the median and the 16th and 84th percentiles of the posterior PDF are plotted above the marginalised PDF.

uncertainties in the estimates of σ_2/σ_1. For instance, Nesti & Salucci (2013, and references therein) claimed that the ratio between low- and high-α sequence stars should be around ten. On the other hand, Fuhrmann et al. (2017) derived a local mass density ratio between thin and thick disc stars of 5.26, which becomes as low as 1.73 after correction for the difference in the scale height. While studying APOGEE stars, Mackereth et al. (2017) found that the relative contribution of low- to high-α is 5.5. Bearing in mind these uncertainties, we set a uniform prior on the mass density ratio, exploring the range $1 < \sigma_2/\sigma_1 < 50$ (assuming that the low-α component is more massive than the high-α one).

Finally, we sampled the posterior probability distribution defined by Eq. (5) using an affine invariant MCMC ensemble sampler (Goodman & Weare 2010; Foreman-Mackey et al. 2013). This was accomplished using the publicly available code "*emcee*: the mcmc hammer"[1]. We initialised the chains with 100 walkers and ran the sampler for 1000 steps (see below for the details).

In this section we also test the method showing results when model free parameters are constrained simply by chemical abundance ratios, that is, the likelihood calculation is based only on [α/Fe] and [Fe/H] abundance ratio data. We recall that in ES19, the presence of a significant delay between the two infall episodes (~4.3 Gyr) was a crucial assumption to properly reproduce the APOKASC data.

We consider three free model parameters: the infall timescales of accretion τ_1 (first gas infall), τ_2 (second infall), and the delay t_{max} between the start of the two infall episodes. The SFE was fixed to the value of $\nu = 1.3\,\mathrm{Gyr}^{-1}$, whereas the present-day surface gas density of the high- and low-α sequences are 8 $M\odot\,\mathrm{pc}^{-2}$ and 64 $M\odot\,\mathrm{pc}^{-2}$, respectively, as suggested by the ES19 best model adopting Nesti & Salucci (2013) prescriptions.

[1] https://emcee.readthedocs.io/en/stable/; https://github.com/dfm/emcee

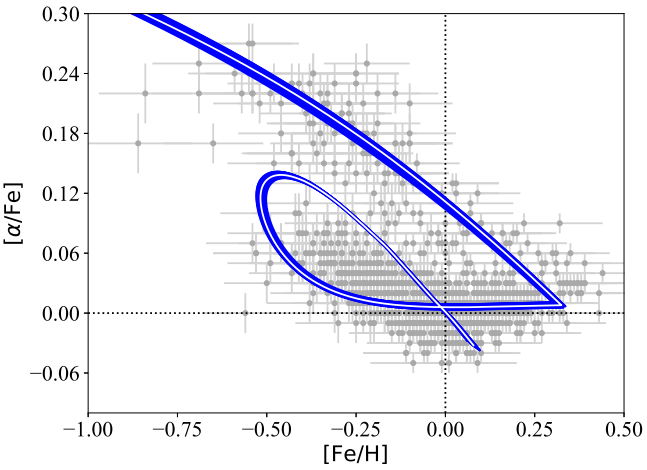

Fig. 4. Observed [α/Fe] vs. [Fe/H] abundance ratios presented by Silva Aguirre et al. (2018, grey points), compared with model results constrained only by abundance ratio data with three free parameters, composed by the set $\boldsymbol{\Theta} = \{\tau_1,\ \tau_2,\ t_{max}\}$ (see Sect. 4). The blue lines correspond to 100 walkers at the last step, and the thin white line indicates the best-fit model.

It should be noted that the number of steps considered in an MCMC calculation can have a significant impact on the results (Goodman & Weare 2010; Foreman-Mackey et al. 2013). In Fig. 2 we show the evolution of 100 walkers as a function of the number of steps. As it can be seen, the chains have converged already after 200 steps, thus ensuring the robustness of the results. The posterior probability density function (PDF) of the model parameters is presented in Fig. 3. The best-fit model parameters are: $\tau_1 = 0.184^{+0.056}_{-0.052}$ Gyr, $\tau_2 = 10.461^{+0.773}_{-0.703}$ Gyr, and $t_{max} = 4.212^{+0.036}_{-0.034}$ Gyr. In Fig. 4 we show the abundance ratios [α/Fe] versus [Fe/H] predicted by 100 walkers computed at the

Table 1. Observed solar chemical abundances compared with the theoretical ones predicted by the best models M1, M2, and M3 (see text for model details) constrained by chemical-abundance ratios and stellar ages of the APOKASC sample.

Abundance log(X/H)+12	Observations Asplund et al. (2005) [dex]	Models M1 [dex]	M2 [dex]	M3 [dex]
Fe	7.45±0.05	7.31	7.31	7.33
Si	7.51±0.04	7.41	7.40	7.42
Mg	7.53±0.09	7.44	7.43	7.45

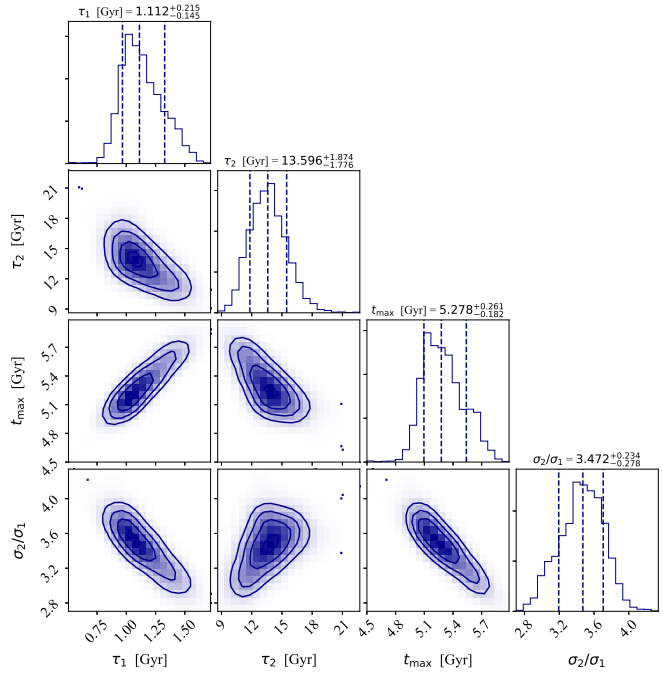

Fig. 5. Corner plot showing the posterior PDFs of model M1 in which the SFE has been fixed at the value of $\nu = 1.3\,\mathrm{Gyr}^{-1}$. In this case the best fit of the 4D parameter space $\boldsymbol{\Theta} = \{\tau_1, \tau_2, t_{\max}, \sigma_2/\sigma_1\}$ is obtained by fitting [α/Fe], [Fe/H], and the ages of the APOKASC sample (see model details in Sect. 5). The median, 16th and 84th percentiles of the posterior PDF are plotted for each parameter above the marginalised PDF.

last time-step of the MCMC steps (at the thousandth step). In this plot the thickness of the model curve represents the uncertainty.

In Fig. 4 we notice that the best model is similar to the one of ES19 (see their Fig. 2), and the associated "loop" feature in the [α/Fe] and [Fe/H] space related to the low-α sequence is retained. The newly constrained free parameter values by the MCMC algorithm are similar to the ones of ES19, and we obtain an almost identical value for the delay $t_{\max}$ with a difference of $\Delta t_{\max} = 0.088$ Gyr.

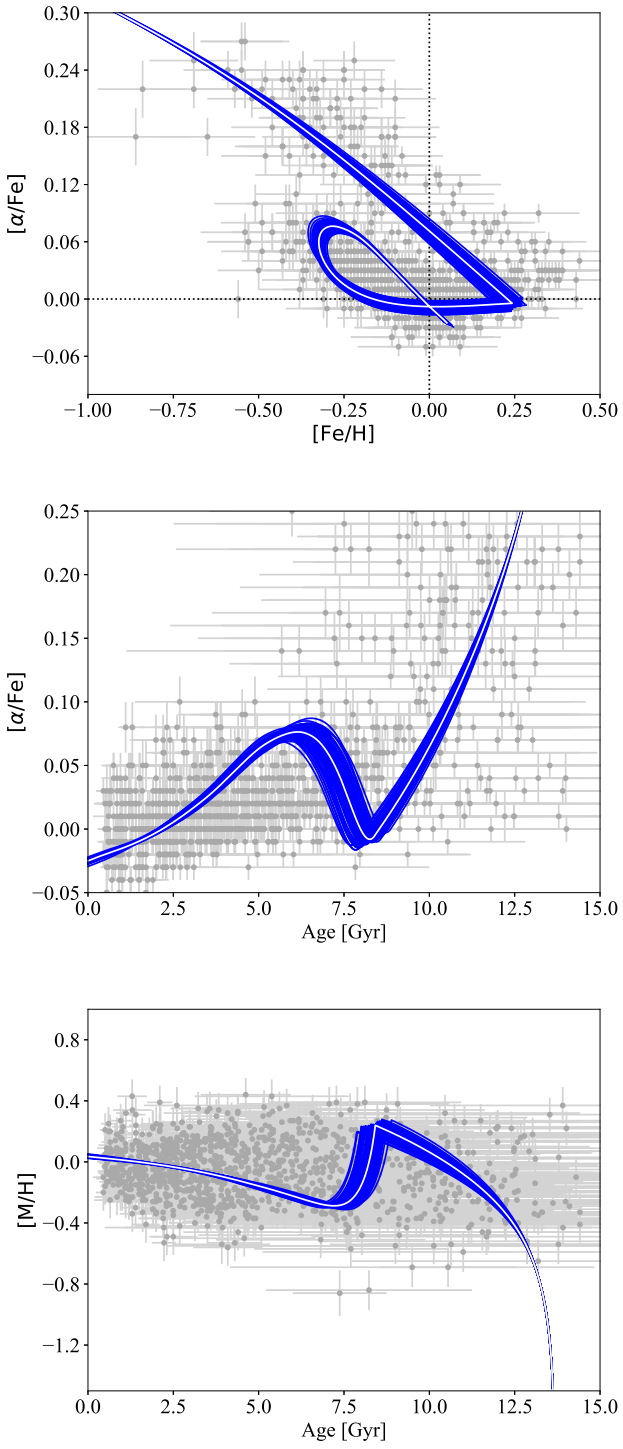

Fig. 6. *Upper panel*: same as Fig. 4 except that the model M1 is also constrained by means of the APOKASC stellar ages. The best-fit model parameters of the set $\boldsymbol{\Theta} = \{\tau_1, \tau_2, t_{\max}, \sigma_2/\sigma_1\}$ were computed by means of the PDFs of Fig. 5. *Middle and lower panel*: temporal evolution of [α/Fe] and age–metallicity relation, respectively, for the same models and data of the upper panel.

5. Results

In this section we show model predictions in the presence of the new dimension provided by asteroseismology, i.e. precise stellar ages. The free parameters are determined by fitting [α/Fe], [Fe/H], and stellar ages provided by the APOKASC sample. We note that, in this analysis, we do not assume the disc component dissection between high-α and low-α stellar sequences by Silva Aguirre et al. (2018) based on the chemistry.

It should be noted that the total surface mass density is another important local key observable. McKee et al. (2015) suggested that the total surface density including the thin and thick components in the solar neighborhood should be

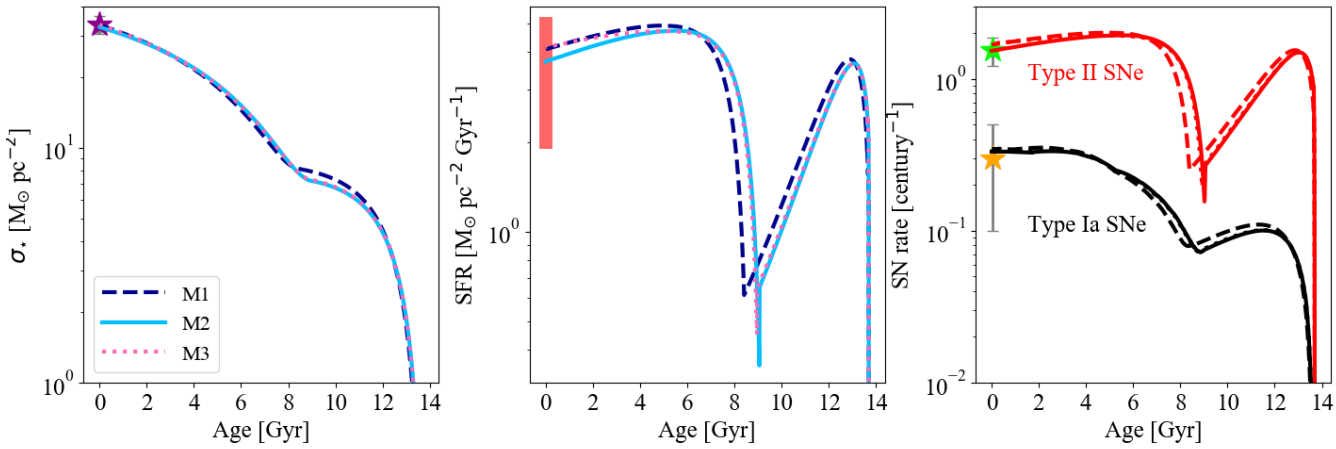

Fig. 7. *Left panel*: stellar surface mass density $\sigma_\star$ evolution predicted by the best-fit models M1 (long dashed line), M2 (solid line), and M3 (dotted line). The purple star indicates the observed present-day value given by McKee et al. (2015). *Middle panel*: same as the left panel for SFR time evolution. The red shaded area indicates the measured range in the solar annulus suggested by Prantzos et al. (2018). *Right panel*: evolution of the Type Ia SN (black lines) and Type II SN (red lines) rates predicted by models M1, M2, and M3 for the whole Galactic disc. The yellow star stands for the observed Type Ia SN rate observed by Cappellaro et al. (1997), whereas the green one stands for Type II SN rates observed by Li et al. (2011).

$47.1 \pm 3.4\, M_\odot$ pc^{-2} and that the total local surface density of stars is $33.4 \pm 3\, M_\odot$ pc^{-2}. In this study, we use the value of total surface density (sum of high-α and low-α) of $47.1 \pm 3.4\, M_\odot$pc^{-2} as provided by McKee et al. (2015) because they also quote a constraint on the stellar mass content.

In contrast to Spitoni et al. (2019a), we do not impose the present-day total low-α sequence surface density (see Eq. (3)) but instead use the total surface mass densities ($\sigma_{\rm tot} = \sigma_1 + \sigma_2$) for consistency as given by the McKee et al. (2015) study. Recalling that σ_2/σ_1 is the ratio between the low-α and high-α present-day total surface mass density, we have

$$\sigma_{\rm tot} = \sigma_2 \left(1 + \frac{1}{\sigma_2/\sigma_1}\right). \tag{9}$$

Therefore, the values of the present-day surface densities σ_2 and σ_1 to insert in Eqs. (3) and (2), respectively, are the following:

$$\sigma_2 = \frac{\sigma_{\rm tot}}{\left(1 + \frac{1}{\sigma_2/\sigma_1}\right)} \text{ and } \sigma_1 = \sigma_{\rm tot} - \sigma_2. \tag{10}$$

We consider, as the reference case, the model with the SFE fixed at the value of $\nu = 1.3$ Gyr (model M1) as assumed in ES19 where the predicted solar values for Mg, Fe, and Si were in agreement within one sigma with Asplund et al. (2005) values (see their Table 1). In Fig. 5 we show the corner plot with the posterior PDFs of the model M1 characterised by the four model parameters $\boldsymbol{\Theta} = \{\tau_1,\ \tau_2,\ t_{\rm max},\ \sigma_2/\sigma_1\}$ with priors as introduced in Sect. 4. We still find a significant delay in the start of the second gas infall, which is even larger than the value found in ES19: $t_{\rm max} = 5.278^{+0.261}_{-0.182}$ Gyr. The best model predicts a value of $3.472^{+0.234}_{-0.278}$ for the σ_2/σ_1 ratio. Therefore, our analysis favours the value derived by Fuhrmann et al. (2017), whereas the much larger value suggested by Nesti & Salucci (2013) seems unsuitable to reproduce the APOKASC data. Moreover, in the [α/Fe] versus [Fe/H] space, this model presents results definitely in agreement with the finding of ES19. Based on a statistical method, we have full confirmation of a significant delay between the two infall episodes, as shown in Fig. 6.

We can see from Table 1 that model M1 predicts Fe solar abundance within 3σ, Si within 2σ, and Mg within 1σ of the observational estimates by Asplund et al. (2005). The model presented in ES19 was able to reproduce solar values for the above-mentioned elements within 1σ. Now we predict smaller solar values compared to ES19 ones because of the longer best-fit timescales of accretion: i.e. $\tau_1 = 1.112^{+0.215}_{-0.145}$ Gyr (first infall) and $\tau_2 = 13.596^{+1.874}_{-1.776}$ Gyr (second infall). Therefore, the chemical enrichment for the model M1 is less efficient and evolves slower in time, leading to smaller solar values compared to ES19.

We also notice that the "loop" in the low-α sequence does not cover all data. We remind the reader that we are considering a model designed for the solar neighborhood and we do not include stellar migration effects. In principle, stellar migration (Schönrich & Binney 2009) can help in reproducing the low-α sequence composed by stars with the smallest [Fe/H] values (with stars migrating into the solar neighbourhood from the outer disk), as well as with the largest [Fe/H] values (with stellar migration from inner disc regions).

In Fig. 6, the temporal evolution of the [α/Fe] shows an evident "bump" and the age–metallicity [M/H][2] relation shows a sudden "drop", both signatures of the delayed infall of gas in agreement with ES19 predictions. The presence of such features is not obvious in the observations but could be hidden behind the observational uncertainties. Here we have tested that Bayesian methods lead to best models characterised by significant delay and important gas dilution.

We note that [α/Fe] values for the youngest stars tend to fall above the predicted [α/Fe] vs. age trend. The predicted slope of the [α/Fe] versus age relation for the low-α disc is similar to the one presented by Chiappini et al. (2015) and moreover agrees better with the trend found by Nissen (2016) for solar twin stars in the solar neighborhood than with the APOKASC data.

An important constraint for the chemical evolution model is the present-time stellar surface mass density. The left panel of Fig. 7 shows that our best model predicts a value of $33.28\, M_\odot$ pc^{-2}, in excellent agreement with the value of

[2] In the age–metallicity relation, the metallicity [M/H] is computed using the expression introduced by Salaris et al. (1993), as done in ES19 to be consistent with the APOKASC sample:

$$[\mathrm{M/H}] = [\mathrm{Fe/H}] + \log\left(0.638 \times 10^{[\alpha/\mathrm{Fe}]} + 0.362\right). \tag{11}$$

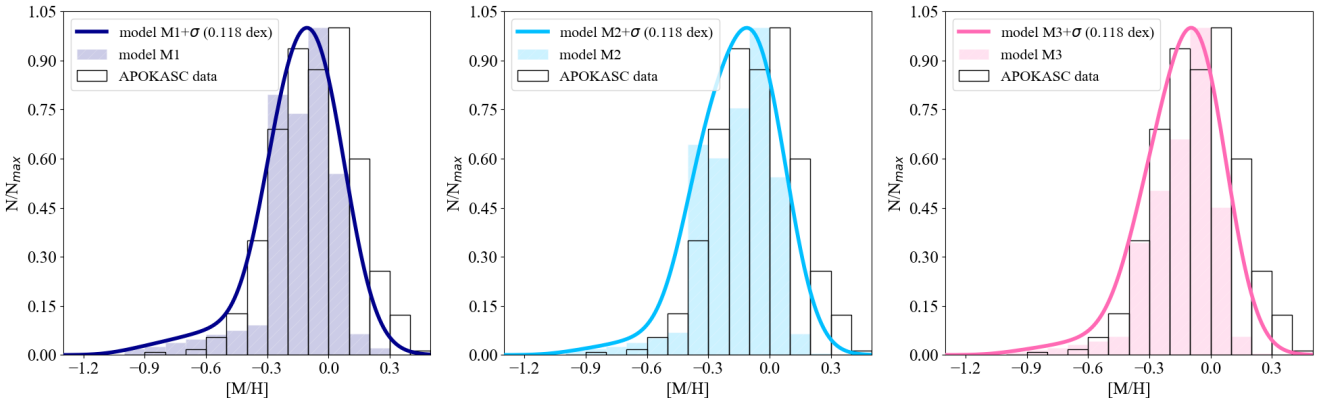

Fig. 8. Metallicity distributions predicted by models M1 (*left panel*), M2 (*middle panel*), and M3 (*right panel*) with the best-fit model parameters (colored histograms). The observed APOKASC distribution calculated including both high-α and low-α stars is shown by the black empty histograms. The solid lines indicate the metallicity distribution of our chemical evolution models convolved with a Gaussian with standard deviation $\sigma = 0.118$ dex (average APOKASC data error). In each plot the distributions are normalised to the corresponding maximum number of stars $N_{\rm max}$.

Table 2. Predicted delay $t_{\rm max}$, present-day surface density ratio σ_2/σ_1, and infall timescale τ_1 values by the models M1, M2, and M3 presented in this work (see text for model details).

	Models			
	M1	M2	M3	
ν_1 [Gyr^{-1}]	1.3	2.0	2.0	
ν_2 [Gyr^{-1}]	1.3	1.0	1.3	
		MCMC results		Range
$t_{\rm max}$ [Gyr]	$5.278^{+0.261}_{-0.182}$	$4.624^{+0.135}_{-0.099}$	$4.721^{+0.126}_{-0.109}$	4.525 – 5.539
σ_2/σ_1	$3.472^{+0.234}_{-0.278}$	$4.176^{+0.167}_{-0.178}$	$4.106^{+0.166}_{-0.165}$	3.194 – 4.334
τ_1 [Gyr]	$1.112^{+0.215}_{-0.145}$	$1.264^{+0.119}_{-0.090}$	$1.295^{+0.119}_{-0.095}$	0.967 – 1.414
τ_2 [Gyr]	$13.596^{+1.874}_{-1.776}$	$11.282^{+0.954}_{-0.943}$	$18.811^{+2.598}_{-2.062}$	10.339 – 21.409

Notes. In the last column, we also provide the range values admitted by our study. The assumed values for high-α (ν_1) and low-α (ν_2) SFEs for the different models are also indicated.

$33.4 \pm 3\,M_\odot\,{\rm pc}^{-2}$ proposed by McKee et al. (2015). From the middle panel of Fig. 7 we notice that the predicted present-day SFR value of $4.08\,M_\odot\,{\rm pc}^{-2}\,{\rm Gyr}^{-1}$ is in agreement with the measured range in the solar vicinity of $2{-}5 M_\odot\,{\rm pc}^{-2}\,{\rm Gyr}^{-1}$ (Matteucci 2012; Prantzos et al. 2018).

The time evolution of the Type Ia SN and Type II SN rates are also plotted in Fig. 7. The present-day Type II SN rate in the whole Galactic disc predicted by our model is 1.67 /[100 yr], in good agreement with the observations of Li et al. (2011) which yield a value of 1.54 ±0.32 /[100 yr]. The predicted present-day Type Ia SN rate in the whole Galactic disc is 0.34 /[100 yr], again in good agreement with the value provided by Cappellaro et al. (1997) of 0.30±0.20 /[100 yr].

In the left panel of Fig. 8 we compare the metallicity distribution function (MDF) of the model M1 with the whole APOKASC data sample. Although the predicted MDF is consistent with the data, it underestimates the number of stars at super-solar metallicities. This is due to the longer best-fit timescales of accretion compared to the classical two-infall model. In Fig. 8 we also draw the curve related to the model distribution convolved with a Gaussian with a constant dispersion fixed at the value of $\sigma = 0.118$ dex, which is the average [M/H] observational error in APOKASC data (see ES19). In this case we improve the fit and the high-metallicity tail of the MDF is better accounted for.

In the following section we test how the delay between the two infall episodes is sensitive to the choice of the SFE parameter.

5.1. Star formation efficiency parameter study (models M2 and M3)

In this section we consider different SFE values as already used in previous works. Different infall episodes could in principle be characterised by different SFEs as suggested by Grisoni et al. (2017, 2018). In their chemical evolution models, the SFEs of the high-α and low-α sequences have been fixed at the values of $\nu_1 = 2\,{\rm Gyr}^{-1}$ and $\nu_2 = 1\,{\rm Gyr}^{-1}$, respectively.

In model M2 we adopt the same prescriptions as Grisoni et al. (2017, 2018) as shown in Table 2, whereas in model M3 we consider $\nu_1 = 2\,{\rm Gyr}^{-1}$ and $\nu_2 = 1.3\,{\rm Gyr}^{-1}$ (high-α SFE as Grisoni et al. 2017 and low-α one as ES19).

In Fig. 9 the corner plot of the posterior PDFs of model M2 confirms the trend mentioned above with model M1. The best value for the time delay is $t_{\rm max} = 4.624^{+0.135}_{-0.099}$ Gyr, and $\sigma_2/\sigma_1 = 4.176^{+0.167}_{-0.178}$. This shows that the timescales of accretion τ_1 and τ_2 are sensitive to the assumed SFE. During the high-α phase, the best model M2 is characterised by a longer timescale τ_1 than that of model M1. In order to obtain a chemical enrichment history similar to that of the M1 model, an increase of the SFE must be

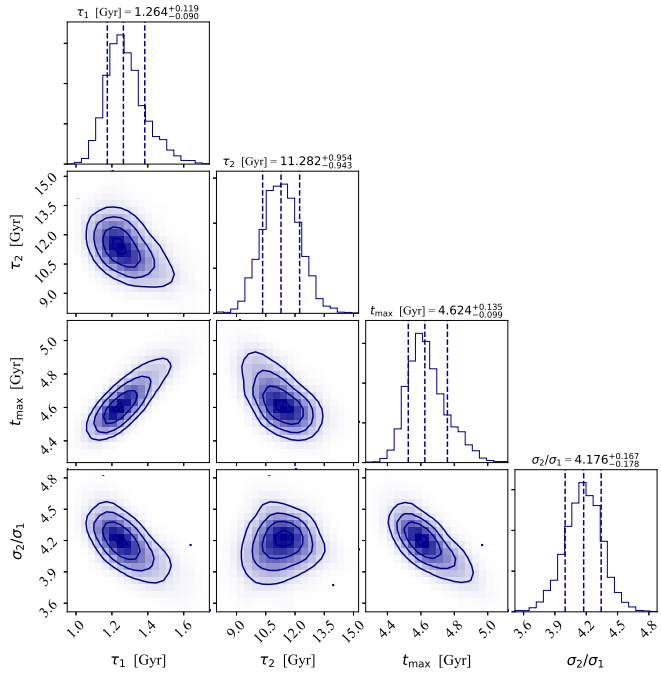

Fig. 9. Corner plot showing the posterior PDFs of model M2 in which we adopt different SFEs for the high-α and low-α sequences: $\nu_1 = 2\,\mathrm{Gyr}^{-1}$ and $\nu_2 = 1\,\mathrm{Gyr}^{-1}$. The best fit of the 4D parameter space $\boldsymbol{\Theta} = \{\tau_1, \tau_2, t_{max}, \sigma_2/\sigma_1\}$ is obtained by fitting [α/Fe], [Fe/H] and ages of the APOKASC sample (see model details in Sect. 5.1). The median, 16th and 84th percentiles of the posterior PDF are plotted for each parameter above the marginalised PDF.

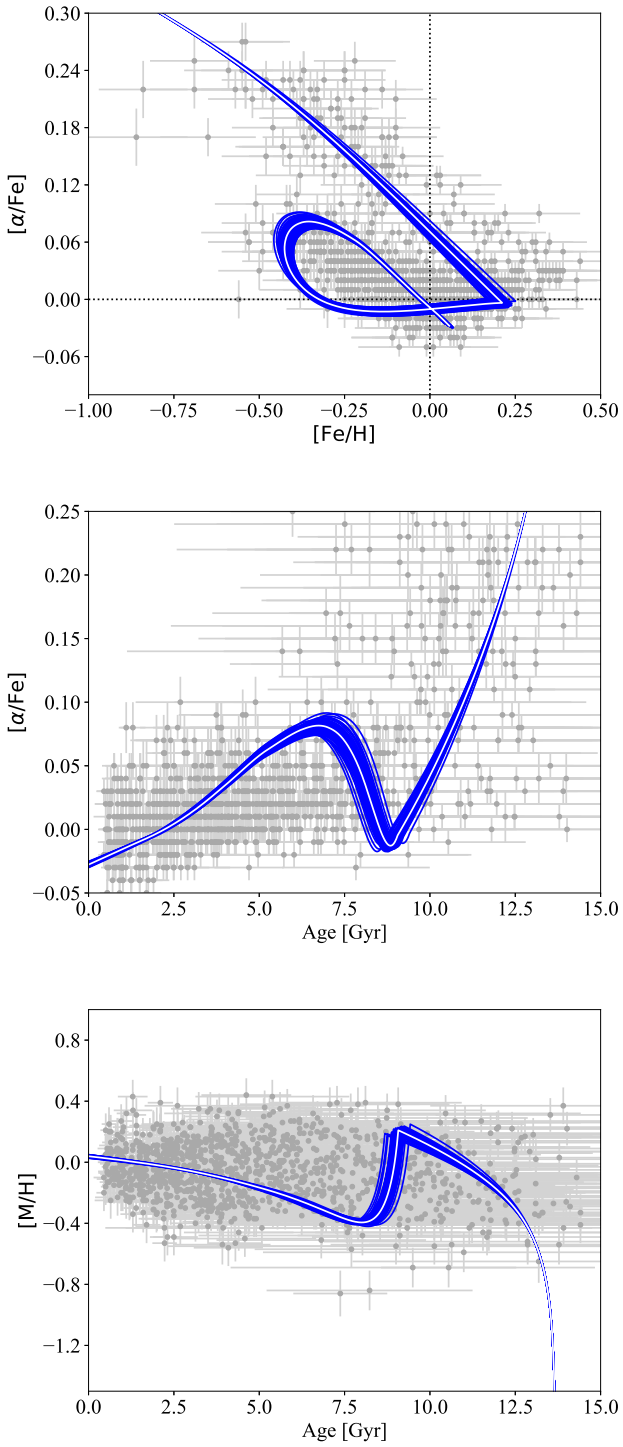

Fig. 10. Same as Fig. 6 for model M2 (see in Sect. 5.1).

compensated by a longer timescale τ_1; the same applies to the second infall timescale.

In Fig. 10, it also is possible in this case to see the dilution effect of the gas rich accretion events in the [α/Fe] versus [Fe/H] abundance ratios, in the age metallicity relation, and in [α/Fe] versus age plot. By comparing Fig. 10 with Fig. 6 we note that the two models show similar results.

An important constraint for the chemical-evolution model is represented by the present-time stellar-surface mass density. The left panel of Fig. 7 shows that our best model M2 predicts a present-time stellar surface mass density value of $32.60\,M_\odot\,\mathrm{pc}^{-2}$, which is slightly smaller than the value proposed by McKee et al. (2015). The predicted present-day SFR value of $3.72\,M_\odot\,\mathrm{pc}^{-2}\,\mathrm{Gyr}^{-1}$ is smaller than the one predicted by the M1 model, in better agreement with the observed range of $2{-}5\,M_\odot\,\mathrm{pc}^{-2}\,\mathrm{Gyr}^{-1}$ (Matteucci 2012; Prantzos et al. 2018).

The present-day Type Ia and II SN rates are also shown in Fig. 7. The present-day Type II SN rate in the whole Galactic disc predicted by our model is 1.53 /[100 yr], in good agreement with the observations by Li et al. (2011). The predicted present-day Type Ia SN rate in the whole Galactic disc is 0.33 /[100 yr], in good agreement with the value provided by Cappellaro et al. (1997).

In the middle panel of Fig. 8 we show the MDF for the model M2. We note that the convolution of the MDF with a Gaussian of standard deviation equal to the typical [M/H] error in the APOKASC sample helps in reproducing the high- and low-metallicity tails of the observed distribution. Because of the larger SFE value for the high-α sequence ν_1, model M2 presents an MDF with more metal-poor stars compared to model M1.

Finally, we present the results related to model M3 characterised by the following SFEs for the two gas infall episodes: $\nu_1 = 2\,\mathrm{Gyr}^{-1}$ and $\nu_2 = 1.3\,\mathrm{Gyr}^{-1}$. The corner plot related to model M3 can be found in Fig. 11. The main difference between model M2 and model M3 is the timescale of accretion of the second infall τ_2; in fact the best-fit model M3 requires $\tau_2 = 18.811^{+0.126}_{-0.109}$ Gyr. However, as can be inferred from Figs. 7, 8, and 12, no substantial differences characterise the chemical enrichment of the model M3 compared to models M1 and M2. The model M3 shows slightly larger solar abundance values (see Table 1) because of the higher SFEs in both high-α and low-α sequences.

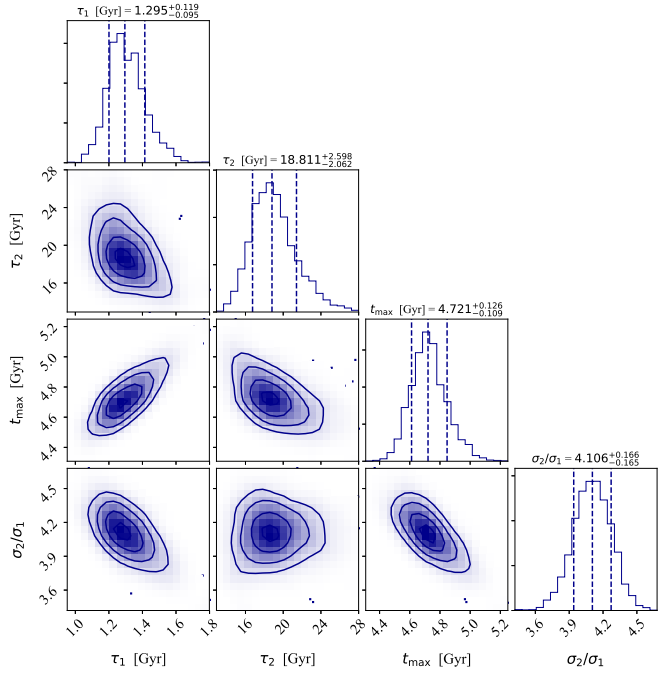

Fig. 11. Corner plot showing the posterior PDFs of model M3 in which we adopt different SFEs for the high-α and low-α sequences: $\nu_1 = 2\,\mathrm{Gyr}^{-1}$ and $\nu_2 = 1.3\,\mathrm{Gyr}^{-1}$ (see model details in Sect. 5.1). The median, 16th and 84th percentiles of the posterior PDF are plotted for each parameter above the marginalised PDF.

In Table 2 we summarise the predicted delay t_{max}, present-day surface-density ratio σ_2/σ_1, and infall timescales τ_1 and τ_2, that is, the values obtained for the different best-fit models presented in this work. In all our tests, independently of the SFE prescription, there is robust evidence for the presence of a delay; its value spans the range 4.5−5.5 Gyr. Another important result is that we are capable of constraining the ratio σ_2/σ_1. The predicted values are in the range 3.2−4.3, in agreement with Fuhrmann et al. (2017) and Mackereth et al. (2017).

The predicted values for τ_1, t_{max}, and σ_2/σ_1 are relatively insensitive to different SFE prescriptions, confirming the robustness of the results. However, the best-fit accretion timescale τ_2 spans a large range of values (10.3–21.4 Gyr) considering models M1, M2, and M3. Therefore, we cannot draw any firm conclusions about this parameter assuming only the observational constraints given by abundance ratios and ages of the APOKASC sample stars.

The predicted timescales for the low-α sequence are substantially longer than the one proposed by the classical two-infall model by Chiappini et al. (2001) and Grisoni et al. (2018) for the solar neighborhood. In these works the "inside-out" formation scenario was obtained with an infall timescale for the thin disc that increases with Galactocentric distance, and in particular in the solar neighborhood $\tau_2 = 7$ Gyr (3.3 Gyr shorter than our lower limit predictions). However, the best fit "low-α" timescales of accretions for models M1 and M2 are in agreement with the chemical evolution model proposed by Nidever et al. (2014). More precisely, originally designed to reproduce the APOGEE data, this model is characterised by an e-folding timescale of gas accretion fixed at the value of 14 Gyr.

In a future study, it is our intention to extend our results to other Galactocentric distances, analysing the inside-out Galactic disc growth, with the inclusion of other observational constraints in the MCMC procedure.

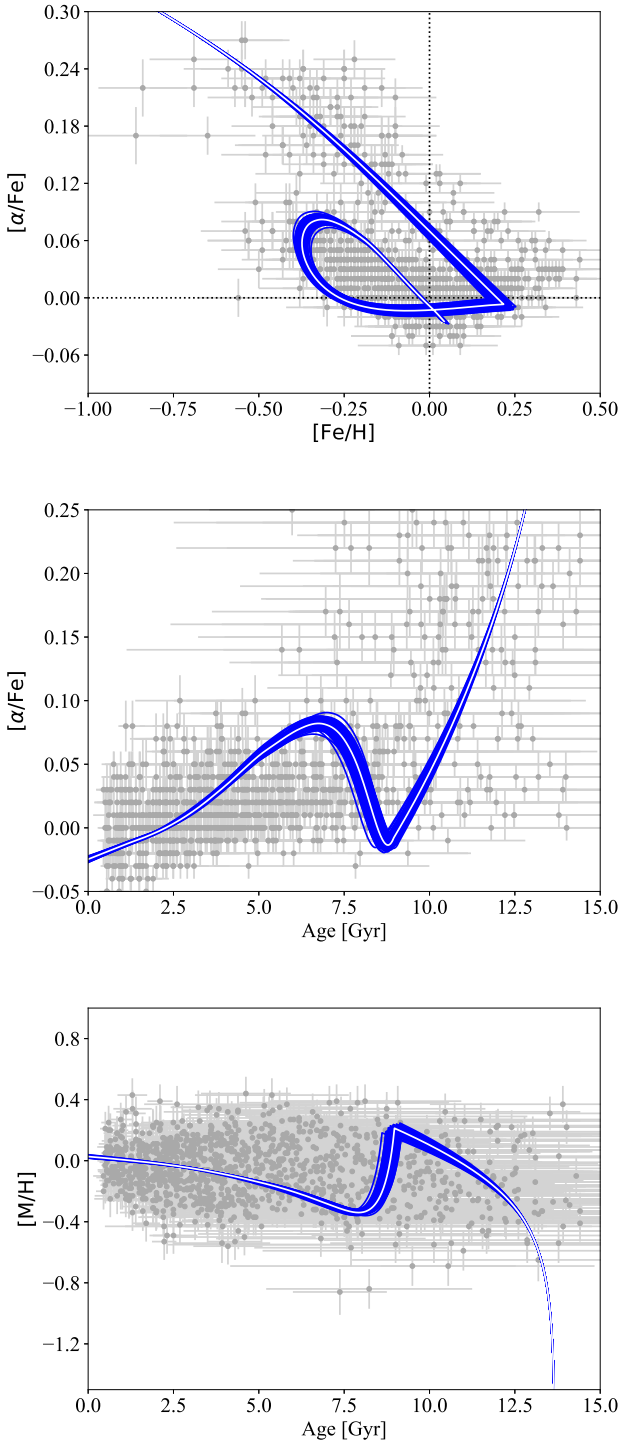

Fig. 12. Same as Fig. 6 but for model M3 with SFEs fixed at the values of $\nu_1 = 2\,\mathrm{Gyr}^{-1}$ $\nu_2 = 1.3\,\mathrm{Gyr}^{-1}$ (see model details in Sect. 5.1).

5.2. The dissection of the Galactic disc components

In previous works, the Galactic disc dissection in the solar neighbourhood was based either on chemical tagging or using the kinematics proprieties of the stars (see Silva Aguirre et al. 2018 and references therein). In this section we propose a new method to separate the APOKASC data into high-α and low-α disc components using the results of our best-fit models, M1, M2, and M3. We present a new criterium in which, in addition to the chemical abundance of the stars, we also use their asteroseimic age information.

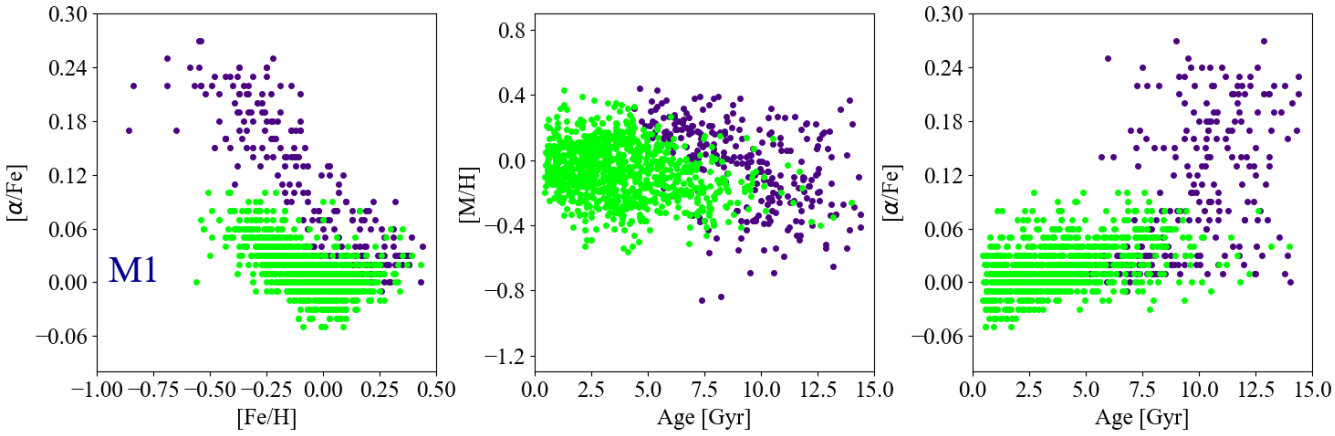

Fig. 13. Disc dissection of the APOKASC sample of Silva Aguirre et al. (2018) in high-α (violet points) and low-α (green points) sequence stars based on the chemical evolution model M1. *Left panel*: abundance ratios [α/Fe] vs. [Fe/H] for the APOKASC sample. The age metallicity relation and the temporal evolution of the [α/Fe] are shown in the *middle and right panels*, respectively.

Given a best-fit model, we associate to each star in the space of observables $\mathbf{x} = \{[\alpha/\mathrm{Fe}],\ [\mathrm{Fe/H}],\ \mathrm{age}\}$, the closest point on the model hyper-surface using Eq. (8) introduced in Sect. 4. If this point on the hyper-surface is characterised by an age that is greater than delay $t_{\max}$, then the star is considered to be part of the high-α sequence. On the other hand, if this age is less than the delay, then it is considered to be part of the low-α sequence.

We find that all the models produce roughly the same disc separation, therefore in Fig. 13 we show only the results obtained with the M1 model. It is interesting to note that this dissection criterium produces a disc separation not much different from the one presented by Silva Aguirre et al. (2018) based on chemistry (see their Fig. 8). However, some relevant differences can be noted in the temporal evolution of the abundance ratio [α/Fe] for old stars with [α/Fe] < 0.05 dex. The dissection based only on chemistry by Silva Aguirre et al. (2018) tags all the stars in this region as low-α sequence. On the other hand, our separation – which uses the age information as well – predicts a mixed population of high-α and low-α stars close to the delay, $t_{\max}$.

By means of a chemo-dynamical model for the Milky Way it will be possible to include also the kinematic information along with the stellar ages and chemical abundances in the Bayesian analysis based on MCMC methods to better constrain the disc dissection and shed more light on the different disc components.

6. Conclusions

For the first time, we used a detailed Bayesian analysis to constrain chemical evolution models with stellar abundances and precise stellar ages provided by asteroseismology of the APOKASC sample by Silva Aguirre et al. (2018). We tested the robustness of the findings of Spitoni et al. (2019a) concerning the importance of a significant delay between the first infall and the start of the second one in the framework of the two-infall chemical evolution model in order to reproduce the APOKASC sample in the solar annulus.

In our analysis we considered four free parameters (accretion time-scales τ_1 and τ_2, delay $t_{\max}$ and present-day surface mass density ratio σ_2/σ_1). We tested three different SFE recipies: in model M1, SFE is fixed at the value of 1.3 Gyr^{-1} during the Galactic life, following Grisoni et al. (2017), and in model M2 and M3 the high-α and low-α sequences are characterised by different SFEs.

Our main conclusions can be summarised as follows:

- The best fit models M1, M2, and M3 present a delay between the two infall episodes in agreement with Spitoni et al. (2019a). These models also reproduce other important observational constraints for the chemical evolution of the disc reasonably well, including the present-day stellar surface density by McKee et al. (2015), Type II and Type Ia SN rates, the SFR, the metallicity distribution function of the APOKASC data, and the solar abundance values of Asplund et al. (2005).
- We show with a Bayesian analysis that the presence of a consistent delay is robust against the uncertainties in the SFEs, and the value lies in the range 4.5−5.5 Gyr for different models.
- The best-fit model parameter for the present-day surface mass–density ratio σ_2/σ_1 between low-α and high-α sequences spans the range 3.2−4.3, which is in agreement with the findings of Fuhrmann et al. (2017).
- We used our best models to dissect the Galactic disc components of the APOKASC sample. The results of the dissection are similar to those presented by Silva Aguirre et al. (2018) based only on chemistry. Differences in the disc separations are for the stars close to the model transaction between high-α and low-α sequences in the [α/FE] versus [Fe/H] space.

Different physical phenomena can be associated to a significant delay in the range 4.5−5.5 Gyr between the two accretion episodes. In the two-infall model scenario coupled with the shock-heating theory, a significant delay between the accretion phases has been suggested also by Noguchi (2018). In their picture, a first infall episode gives rise to the high-α sequence, which is followed by a hiatus until the shock-heated gas in the Galactic dark matter halo has radiatively cooled and can be accreted by the Galaxy. In this framework, Noguchi (2018) found that the SFR of the Galactic disc is characterised by two peaks separated by ∼5 Gyr (in agreement with ES19 and our findings).

The significant delay in the two-infall model of ES19 was also discussed by Vincenzo et al. (2019) in the context of the stellar system accreted by the Galactic halo, *Gaia*-Enceladus (Helmi et al. 2018; Koppelman et al. 2019). Vincenzo et al. (2019) presented the first chemical -evolution model for Enceladus, investigating the star formation history of one of the most massive satellites accreted by the Milky Way during a major merger event. It was proposed that the mechanism that quenched the

Milky Way star formation at high redshift by heating up the gas in the dark matter halo was a major merger event with a satellite like Enceladus. This proposed scenario is in agreement with the recent study by Chaplin et al. (2020) . These latter authors constrained the merging time with the very bright, naked-eye star ν Indi finding that, at 68% confidence, the earliest the merger could have started was 11.6 Gyr ago.

Finally, the delay could be interpreted as the main effect of the late, gas-rich accretion episode that shaped the low-α sequence, which was confirmed in early works of chemical evolution in a cosmological context (Calura & Menci 2009) and more recently by cosmological simulations (Buck 2020). We are aware that our study is limited to the solar annulus region, and that other dynamical processes such as stellar migration (Schönrich & Binney 2009) might have played an important role during the Galactic evolution.

Acknowledgements. The authors thank the anonymous referee for various suggestions that improved the paper. Funding for the Stellar Astrophysics Centre is provided by The Danish National Research Foundation (Grant agreement no.: DNRF106). E. Spitoni thanks P. E. Nissen, A. Saro and M. Fredslund Andersen for useful discussions. E. Spitoni and V. Silva Aguirre acknowledge support from the Independent Research Fund Denmark (Research grant 7027-00096B).

References

Asplund, M., Grevesse, N., & Sauval, A. J. 2005, in Cosmic Abundances as Records of Stellar Evolution and Nucleosynthesis, eds. T. G. Barnes, III., & F. N. Bash, ASP Conf. Ser., 336, 25
Belfiore, F., Vincenzo, F., Maiolino, R., & Matteucci, F. 2019, MNRAS, 487, 456
Borucki, W., Koch, D., Batalha, N., et al. 2009, in Transiting Planets, eds. F. Pont, D. Sasselov, & M. J. Holman, IAU Symp., 253, 289
Brooks, S., Gelman, A., Jones, G., & Meng, X.-L. 2011, Handbook of Markov Chain Monte Carlo (CRC Press)
Buck, T. 2020, MNRAS, 491, 5435
Calura, F., & Menci, N. 2009, MNRAS, 400, 1347
Cappellaro, E., & Turatto, M. 1997, in NATO Advanced Science Institutes (ASI) Series C, eds. P. Ruiz-Lapuente, R. Canal, & J. Isern , 486, 77
Cescutti, G., Matteucci, F., François, P., & Chiappini, C. 2007, A&A, 462, 943
Cescutti, G., Hirschi, R., Nishimura, N., et al. 2018, MNRAS, 478, 4101
Chaplin, W. J., Serenelli, A. M., Miglio, A., et al. 2020, Nat. Astron., in press [arXiv:2001.04653]
Chiappini, C., Matteucci, F., & Gratton, R. 1997, ApJ, 477, 765
Chiappini, C., Matteucci, F., & Romano, D. 2001, ApJ, 554, 1044
Chiappini, C., Anders, F., Rodrigues, T. S., et al. 2015, A&A, 576, L12
Côté, B., O'Shea, B. W., Ritter, C., Herwig, F., & Venn, K. A. 2017, ApJ, 835, 128
Dunkley, J., Bucher, M., Ferreira, P. G., Moodley, K., & Skordis, C. 2005, MNRAS, 356, 925
Foreman-Mackey, D., Hogg, D. W., Lang, D., & Goodman, J. 2013, PASP, 125, 306
François, P., Matteucci, F., Cayrel, R., et al. 2004, A&A, 421, 613
Frankel, N., Rix, H.-W., Ting, Y.-S., Ness, M., & Hogg, D. W. 2018, ApJ, 865, 96
Fuhrmann, K., Chini, R., Kaderhandt, L., & Chen, Z. 2017, MNRAS, 464, 2610
Gaia Collaboration (Brown, A.G.A., et al.) 2016, A&A, 595, A2
Gaia Collaboration (Katz, D., et al.) 2018, A&A, 616, A11
García Pérez, A. E., Allende Prieto, C., Holtzman, J. A., et al. 2016, AJ, 151, 144
Gelman, A., Carlin, J., Stern, H., et al. 2013, Bayesian Data Analysis, 3rd edn., Chapman & Hall/CRC Texts in Statistical Science (Taylor & Francis)
Goodman, J., & Weare, J. 2010, Appl. Math. Comput. Sci., 5, 65
Grand, R. J. J., Bustamante, S., Gómez, F. A., et al. 2018, MNRAS, 474, 3629
Grisoni, V., Spitoni, E., Matteucci, F., et al. 2017, MNRAS, 472, 3637
Grisoni, V., Spitoni, E., & Matteucci, F. 2018, MNRAS, 481, 2570
Hayden, M. R., Bovy, J., Holtzman, J. A., et al. 2015, ApJ, 808, 132
Helmi, A., Babusiaux, C., Koppelman, H. H., et al. 2018, Nature, 563, 85
Henriques, B. M. B., Thomas, P. A., Oliver, S., & Roseboom, I. 2009, MNRAS, 396, 535
Henriques, B. M. B., White, S. D. M., Thomas, P. A., et al. 2013, MNRAS, 431, 3373
Hogg, D. W., & Foreman-Mackey, D. 2018, ApJS, 236, 11
Jaynes, E. T. 2003, Probability Theory: The Logic of Science (Cambridge University Press: Cambridge)
Jofré, P., Jorissen, A., Van Eck, S., et al. 2016, A&A, 595, A60
Kampakoglou, M., Trotta, R., & Silk, J. 2008, MNRAS, 384, 1414
Kennicutt, Jr., R. C. 1998, ApJ, 498, 541
Koppelman, H. H., Helmi, A., Massari, D., Price-Whelan, A. M., & Starkenburg, T. K. 2019, A&A, 631, L9
Li, W., Chornock, R., Leaman, J., et al. 2011, MNRAS, 412, 1473
Lindegren, L., Lammers, U., Bastian, U., et al. 2016, A&A, 595, A4
Mackereth, J. T., Bovy, J., Schiavon, R. P., et al. 2017, MNRAS, 471, 3057
Majewski, S. R., Schiavon, R. P., Frinchaboy, P. M., et al. 2017, AJ, 154
Martig, M., Rix, H.-W., Silva Aguirre, V., et al. 2015, MNRAS, 451, 2230
Matteucci, F. 2012, Chemical Evolution of Galaxies (Springer-Verlag Berlin: Heidelberg)
McKee, C. F., Parravano, A., & Hollenbach, D. J. 2015, ApJ, 814, 13
Mikolaitis, S., de Laverny, P., Recio-Blanco, A., et al. 2017, A&A, 600, A22
Mott, A., Spitoni, E., & Matteucci, F. 2013, MNRAS, 435, 2918
Nesti, F., & Salucci, P. 2013, JCAP, 7, 016
Nidever, D. L., Bovy, J., Bird, J. C., et al. 2014, ApJ, 796, 38
Nissen, P. E. 2016, A&A, 593, A65
Noguchi, M. 2018, Nature, 559, 585
Philcox, O., Rybizki, J., & Gutcke, T. A. 2018, ApJ, 861, 40
Pinsonneault, M. H., Elsworth, Y., Epstein, C., et al. 2014, ApJS, 215, 19
Prantzos, N., Abia, C., Limongi, M., Chieffi, A., & Cristallo, S. 2018, MNRAS, 476, 3432
Putze, A., Derome, L., & Maurin, D. 2010, A&A, 516, A66
Recio-Blanco, A., de Laverny, P., Kordopatis, G., et al. 2014, A&A, 567, A5
Reynolds, C. S., Brenneman, L. W., Lohfink, A. M., et al. 2012, ApJ, 755, 88
Rojas-Arriagada, A., Recio-Blanco, A., de Laverny, P., et al. 2016, A&A, 586, A39
Rojas-Arriagada, A., Recio-Blanco, A., de Laverny, P., et al. 2017, A&A, 601, A140
Rybizki, J., Just, A., & Rix, H.-W. 2017, A&A, 605, A59
Salaris, M., Chieffi, A., & Straniero, O. 1993, ApJ, 414, 580
Salaris, M., Cassisi, S., Schiavon, R. P., & Pietrinferni, A. 2018, A&A, 612, A68
Scalo, J. M. 1986, Fund. Cosmic Phys., 11, 1
Schönrich, R., & Binney, J. 2009, MNRAS, 396, 203
Sharma, S. 2017, ARA&A, 55, 213
Silva Aguirre, V., Davies, G. R., Basu, S., et al. 2015, MNRAS, 452, 2127
Silva Aguirre, V., Lund, M. N., Antia, H. M., et al. 2017, ApJ, 835, 173
Silva Aguirre, V., Bojsen-Hansen, M., Slumstrup, D., et al. 2018, MNRAS, 475, 5487
Speagle, J. S. 2019, J. Stat. Edu., submitted [arXiv:1909.12313]
Spitoni, E., & Matteucci, F. 2011, A&A, 531, A72
Spitoni, E., Romano, D., Matteucci, F., & Ciotti, L. 2015, ApJ, 802, 129
Spitoni, E., Gioannini, L., & Matteucci, F. 2017, A&A, 605, A38
Spitoni, E., Silva Aguirre, V., Matteucci, F., Calura, F., & Grisoni, V. 2019a, A&A, 623, A60
Spitoni, E., Cescutti, G., Minchev, I., et al. 2019b, A&A, 628, A38
Ural, U., Wilkinson, M. I., Read, J. I., & Walker, M. G. 2015, Nat. Commun., 6, 7599
Vincenzo, F., Spitoni, E., Calura, F., et al. 2019, MNRAS, L74
Yong, D., Casagrande, L., Venn, K. A., et al. 2016, MNRAS, 459, 487
Zacharias, N., Finch, C. T., Girard, T. M., et al. 2013, AJ, 145, 44